Doping induced anisotropic growth in C_{60}

Miao Miao Wu,[1] Qiang Sun,[1,2,a)] Qian Wang,[2] Puru Jena,[2] and Yoshiyuki Kawazoe[3]
[1]*Department of Advanced Materials and Nanotechnology and Center for Applied Physics and Technology, Peking University, Beijing 100871, China*
[2]*Department of Physics, Virginia Commonwealth University, Richmond, Virginia 23284, USA*
[3]*Institute for Material Research, Tohoku University, Sendai 980-8577, Japan*

(Received 26 February 2009; accepted 22 April 2009; published online 14 May 2009)

Using density functional theory with generalized gradient approximation for exchange and correlation energy, we show that substitution of a Si atom at one of the C sites in C_{60} not only allows $C_{59}Si$ to have a hydrophobic head with a hydrophilic tail but also the Si atom acts as a seed for anisotropic growth of the heterofullerene. This is demonstrated by interacting $C_{59}Si$ with N_7Sc and B_8Si. The resulting complex structures exhibit enhanced electric dipole moments and anisotropy. Thus, doping induced anisotropic growth of nanostructures provides a novel route for the synthesis of bifunctional particles with atomic-level control on selectivity and diversity. These particles may have important applications in biomedical, solar, and display industry. © *2009 American Institute of Physics*. [DOI: 10.1063/1.3134115]

I. INTRODUCTION

Nanoparticles, due to their reduced size, low coordination, low dimensionality, and large surface to volume ratio, possess unique properties that are very different from their bulk. The ability to control the size and composition of nanoparticles has provided scientists the freedom to design new materials with tailored properties. Because of the minimization of the surface tension energy, the nanoparticles typically assume spherical-like shape as exemplified by structures with icosahedric and cuboctahedric symmetry, such as fullerenes. However, recently there has been a growing interest in introducing anisotropy[1–6] to the structure of these isotropic nanoparticles so that they can be bifunctional and have more desirable properties than isotropic materials. De Gennes[7] named these anisotropic nanoparticles after the Roman god Janus who, with two heads, could perform two different tasks at the same time. These bifunctional Janus nanoparticles can have novel applications in molecular recognition, self-assembly, photonic crystals, hydrogen storage, sensors, drug delivery, surfactants, solar cells, and display materials. For example, in biomedical applications the nanoparticles may have one side containing molecules for detection, while the other side can carry the drug. For solar cell applications, one side of the particle can be an electron acceptor, while the other side an electron donor. For use as surfactant materials, one side can be hydrophilic, while the other side is hydrophobic. For paper-thin materials for video displays, a large electric dipole moment will enable the nanoparticles to be manipulated by an applied external electric field. These fascinating applications have stimulated scientists to devise techniques[8–14] such as electrochemical and photochemical reduction, templating of porous membranes and nanotubes, and surfactant-aided growth for introducing desired anisotropies. However, due to complicated nucleation and growth processes it is difficult to precisely control the size and morphology of these anisotropic particles. Therefore, developing easier techniques for the synthesis of Janus nanostructures has considerable merit.[15,16]

In this article, we have studied Janus nanostructures based on C_{60} fullerenes, which have become the symbol for nanoscience and nanotechnology. In C_{60} all the C atoms are equivalent and arranged in a nearly spherical shape with the highest symmetry (I_h). Its geometry and electronic structures are isotropic; hence C_{60} assembled material has a close packed fcc structure. We show that this symmetry can be broken by replacing one of the C atoms with Si, which then leads to selective and anisotropic growth. The choice of $C_{59}Si$ was made for the following reasons. First it has already been synthesized in experiment.[17] Second, although Si belongs to the same group as C, its chemical behavior is quite different. Note that the chemistry of C is characterized by very flexible bonding features. It is able to form single, double, and triple bonds with itself and with other atoms. However, the larger number of core electrons makes it much more difficult for two Si atoms to form double and triple bonds.[18] Consequently, Si prefers to form multidirectional single bonds (sp^3). This feature is quite obvious in pure Si clusters, which are known to adopt compact three-dimensional structures. Thus, substitutional Si doping would make $C_{59}Si$ heterofullerene more reactive at/near the Si site and hence can preferentially bind to other molecules, leading naturally to Janus-like structures. In the following we describe our computational procedure and discuss the properties of C_{60}, $C_{59}Si$, and its interaction with N_7Sc, B_8Si, and H_2O.

II. COMPUTATIONAL METHODS

The calculations were carried out by using density functional theory (DFT) with generalized gradient approximation for the exchange-correlation energy with the Perdew–Wang

a)Electronic addresses: sunq@coe.pku.edu.cn.

91 form.[19] In order to optimize geometry effectively, a plane-wave basis set is adopted with the projector-augmented-wave (PAW) method originally developed by Blochl[20] and recently adapted by Kresse and Joubert[21] as implemented in the VIENNA AB INITIO SIMULATION PACKAGE. The particular advantage of the PAW method over the ultrasoft pseudopotentials is that the pseudization of the augmentation charge can be avoided. The structure optimization is symmetry unrestricted and carried out using conjugate-gradient algorithm. The convergence for energy and force were set to 0.0005 eV and 0.01 eV/Å, respectively. A supercell approach was used where the clusters under investigation were surrounded by 15 Å of vacuum space along the x, y, and z directions. Due to the large supercell, the Γ point was used to represent the Brillouin zone.

III. RESULTS AND DISCUSSION

In Sec. III A, we deal with the structure and properties of C_{60} and $C_{59}Si$. The structure and properties of N_7Sc and B_8Si clusters used to demonstrate the anisotropic growth pattern of $C_{59}Si$ are discussed in Sec. III B. In Secs. III C and III D we discuss the interaction of $C_{59}Si$ with N_7Sc and B_8Si, respectively. In Sec. III E we discuss the sequential interaction of N_7Sc and B_8Si with $C_{59}Si$. Finally in Sec. III F we describe the interaction of $C_{59}Si$ with H_2O to demonstrate its hydrophobic and hydrophilic properties and how this can be enhanced when the anisotropy is further increased by binding $C_{59}Si$ to (N_7Sc+B_8Si).

A. C_{60} and $C_{59}Si$

We begin our discussion with results on C_{60} and $C_{59}Si$. To validate our theoretical method we have computed the properties of C_{60} and $C_{59}Si$ and compared these with previous calculations and experiments. The calculated average binding energy per atom of C_{60} is 7.651 eV. The highest occupied molecular orbital (HOMO) is fivefold degenerate with h_u symmetry, and the lowest unoccupied molecular orbital (LUMO) is threefold degenerate with t_{1u} symmetry. The HOMO-LUMO gap, the longer C–C bond between a hexagon and a pentagon, and the shorter C–C bond length between the two hexagons are 1.610 eV and 1.452 and 1.398 Å, respectively. These agree well with known values.[22–25]

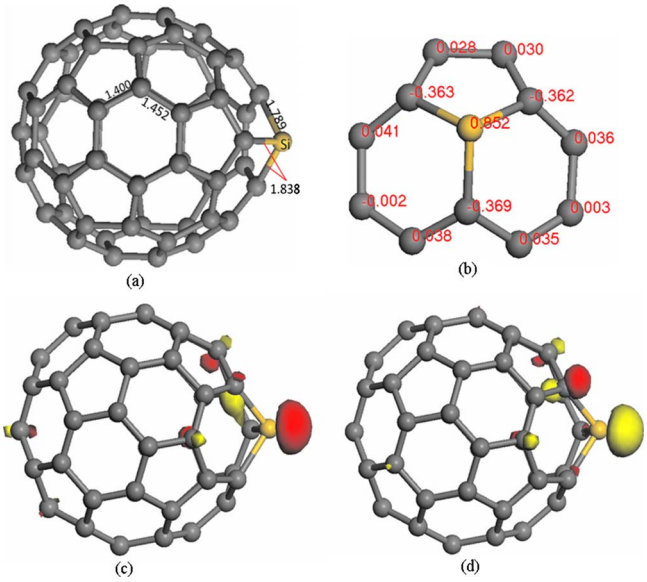

FIG. 1. (Color online) (a) Optimized geometry, (b) Mulliken charge distributions, (c) HOMO, and (d) LUMO of $C_{59}Si$.

The energy cost to replace one C atom with Si is calculated by taking the total energy difference, namely, $\Delta E = E(C_{59}Si) + E(C) - E(C_{60}) - E(Si)$, and is 5.080 eV, in agreement with the existing value of 5.0 eV.[22] The average Si–C bond distance is 1.822 Å, and the symmetry changes from I_h to C_2. The HOMO-LUMO gap is decreased from 1.610 to 1.170 eV. Note that the corresponding value in the Hartree-Fock (HF) approximation is 0.990 eV.[21] Furthermore, the HOMO and LUMO are mainly concentrated on the Si site and its neighboring C sites, as shown in Fig. 1. Because of the difference in electronegativity between C and Si, charge is transferred from Si to C. The Si site carries a positive charge of 0.852, while each of its three neighboring C sites carries an average negative charge of 0.365. This allows $C_{59}Si$ to have a dipole moment of 1.420 D. In Table I, we summarize these results and compare them with available data. From the geometry, charge distribution, and the frontier orbitals, we can clearly see the anisotropy induced by Si doping. The Si site can thus be used as the "seed" for anisotropic growth as ligand molecules are attached.

TABLE I. Bond lengths (d, in angstrom), energy gap (eV) of $C_{59}Si$ and C_{60}, and energy cost ΔE (eV).

	C_{60}[a]	C_{60} (PM3)[b]	C_{60} =[c]	$C_{59}Si$[a]	$C_{59}Si$ (PM3)[b]	$C_{59}Si$ (MD)[d]	$C_{59}Si$ (LDA)[e]
$d_{C-C(5-6)}$	1.452	1.45–1.47	1.46	···	···	···	···
$d_{C-C(6-6)}$	1.398	1.38–1.40	1.39	···	···	···	···
$d_{Si-C(5-6)}$	···	···	···	1.838	1.79	1.90	1.84
$d_{Si-C(6-6)}$	···	···	···	1.789	1.69	1.85	1.75
Energy gap	1.610	···	···	1.170	0.99	1.17	1.20
ΔE	5.080	···	5.00	···	···	···	···

[a]Present work.
[b]Reference 22.
[c]Reference 23.
[d]Reference 24.
[e]Reference 25.

B. N_7Sc and B_8Si

Of many molecules and clusters that we could have used to study the anisotropic growth pattern of $C_{59}Si$, we chose N_7Sc and B_8Si for their unique properties. N_7Sc is a candidate for high energy density materials as the ratio between the energy released in a fragmentation reaction and the specific weight is large. Calculations using DFT and B3LYP functional for exchange and correlation potential as well as MP2 level of theory[26] have revealed that N_7Sc has a local minimum with C_{7v} symmetry and all frequencies are real. Seven N atoms form a ring and Sc atom is capped to the ring as shown in Fig. 2(a_1). The charge analysis reveals that about one electron is transferred to N sites [Fig. 2(b_1)]. The HOMO is mainly contributed by the N ring and the LUMO originates from $3d_{z2}-$Sc [Figs. 2(c_1) and 2(d_1)]. N_7Sc is metastable and dissociates to $Sc+(7/2)N_2$ The dissociation products lie 125 kcal/mol lower in energy[26] than N_7Sc.

B_8Si, on the other hand, is a planar octacoordinate Si with a structure that resembles a molecular wheel[27] [Fig. 2(a_2)]. While planar coordinate C and B clusters have been known, the discovery of similar structure for Si completes a structural transition from molecular fans to a perfect molecular wheel. The planar hypercoordinate silicon atoms with coordination numbers greater than four follow the octet rule by forming partial bonds with surrounding B atoms. Because of the larger electronegativity of B, charges are transferred from Si to B in the molecular wheel [Fig. 2(b_2)]. The HOMO and LUMO are predominantly from B sites [Figs. 2(c_2) and 2(d_2)]. In Table II, we give the calculated parameters and compare with the earlier data.

C. Interaction of N_7Sc with $C_{59}Si$

In this section, we discuss how N_7Sc molecule interacts with $C_{59}Si$. To determine the preferred binding site we designed five different configurations (from $isomer_I$ to $isomer_V$) as starting points in the geometry optimization procedure. These are shown in Fig. 3. In the first one, N_7Sc is directly capped to the Si on the top site. The corresponding adsorption energy, defined as, $\Delta E=-[E(C_{59}Si+N_7Sc)-E(C_{59}Si)-E(N_7Sc)]$, is calculated to be 0.417 eV with Sc–Si distance of 2.892 Å. In this configuration, since both Sc and Si are positively charged [see Figs. 1(b) and 2(b_1)], N_7Sc is weakly adsorbed and the repulsion between Sc and Si results in a larger distance. In the second and third configurations, N_7Sc was placed at the furthest site from Si above the hexagon and pentagon faces, respectively. The corresponding adsorption energies are again weak, namely, 0.427 and 0.473 eV, respectively. We then placed N_7Sc molecule next to the C sites neighboring Si. In the fourth configuration, N_7Sc was placed above C-containing hexagon. The optimized geometry indicates that the positively charged Si site binds to N, while the positively charged Sc binds to C, resulting in strong adsorption energy of 1.739 eV. When we

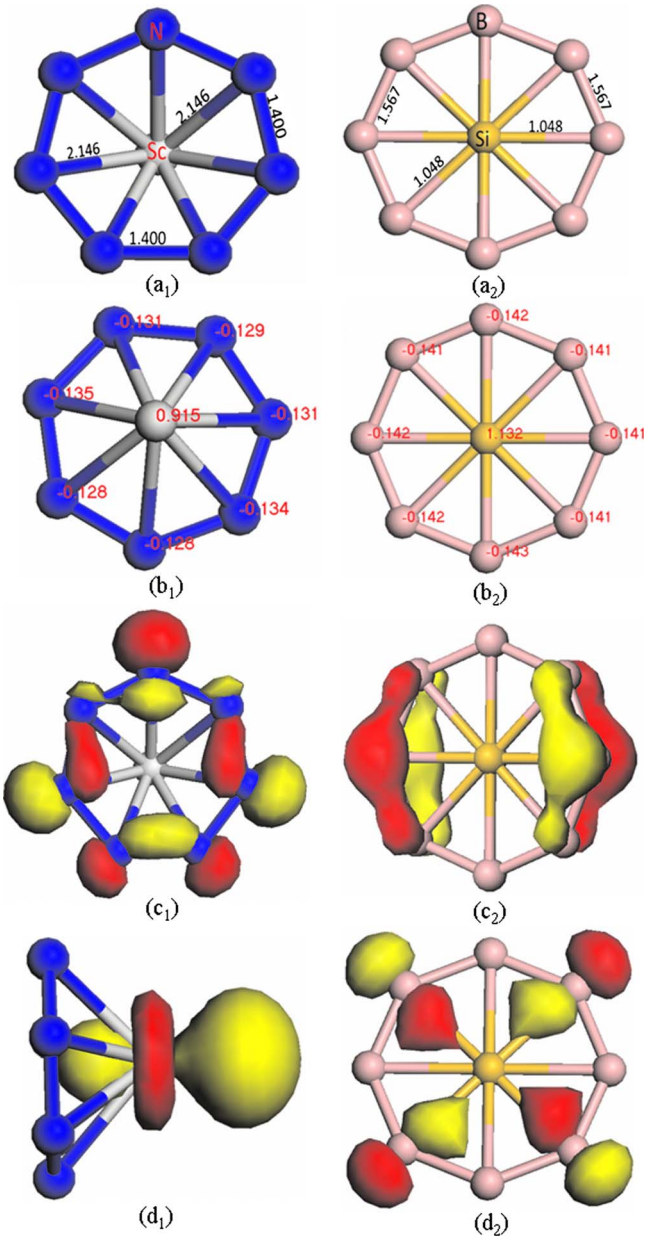

FIG. 2. (Color online) [(a_1) and (a_2)] Relaxed structures, [(b_1) and (b_2)] Mulliken charge distributions, [(c_1) and (c_2)] HOMO, and [(d_1) and (d_2)] LUMO orbitals of N_7Sc and B_8Si, respectively, where (d_1) is rotated in order to better visually appreciate the LUMO.

TABLE II. The calculated distances (in angstrom) between N–N and N–Sc in N_7Sc and between B–B and B–Si in B_8Si.

Bonds	N_7Sc[a]	N_7Sc[b]	Bonds	B_8Si[a]	B_8Si[c]
d_{N-N}	1.400	1.371	d_{B-B}	1.568	1.559
d_{N-Sc}	2.146	2.144	d_{B-Si}	2.046	2.037

[a]Present work.
[b]Reference 26.
[c]Reference 27.

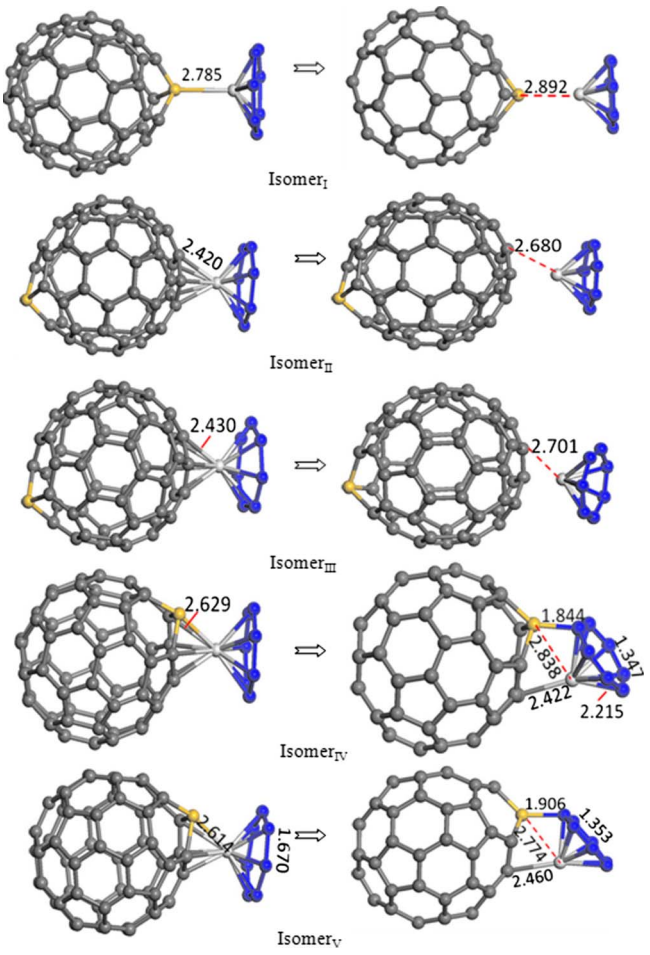

FIG. 3. (Color online) Initial (left column) and optimized (right column) structures of $C_{59}Si+N_7Sc$. All the labeled bond values are in angstrom (Å).

placed N_7Sc on the Si-containing pentagon (see configuration isomer$_V$), it yields a similar geometry but with larger bond lengths and hence a smaller adsorption energy, namely, 1.451 eV.

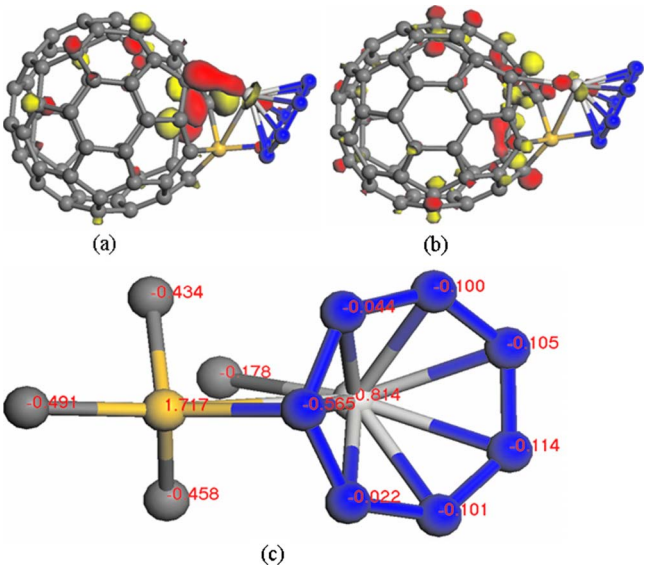

FIG. 4. (Color online) (a) HOMO and (b) LUMO orbitals and (c) Mulliken charges distributions in $C_{59}Si-N_7Sc$ (isomer$_{IV}$).

In order to see the effect of adsorption of N_7Sc on the electronic structure and charge distributions, we plot HOMO and LUMO for the most stable configuration (isomer$_{IV}$) in Fig. 4. We can clearly see that the main contributions to these frontier orbitals come from the C sites neighboring the Si site, the anisotropy is enhanced, and the Si site becomes more positively charged due to the charge transfer to N site. This is reflected in the electric dipole moment of the complex, namely, 2.89 D, which is larger than that of $C_{59}Si$.

D. Interaction of B_8Si with $C_{59}Si$

Following the same procedure as above, we studied the binding of B_8Si with $C_{59}Si$. We again considered five configurations as given Fig. 5. In isomer$_I$, B_8Si, placed on top of Si, yields adsorption energy of 0.790 eV with a Si–B bong length of 2.395 Å. In isomer$_{II}$ and isomer$_{III}$ when the molecule is placed at the opposite end of the Si site, the adsorptions are weak (0.104 eV for on top of hexagon and 0.103 eV for on top of pentagon). However, the adsorption becomes much stronger when the molecule is placed above the Si-containing hexagon (isomer$_{IV}$) or pentagon (isomer$_V$). The corresponding adsorption energies are 1.155 and 1.220 eV, respectively. It is interesting to see that in the ground state configuration (isomer$_V$), the molecular wheel B_8Si is at-

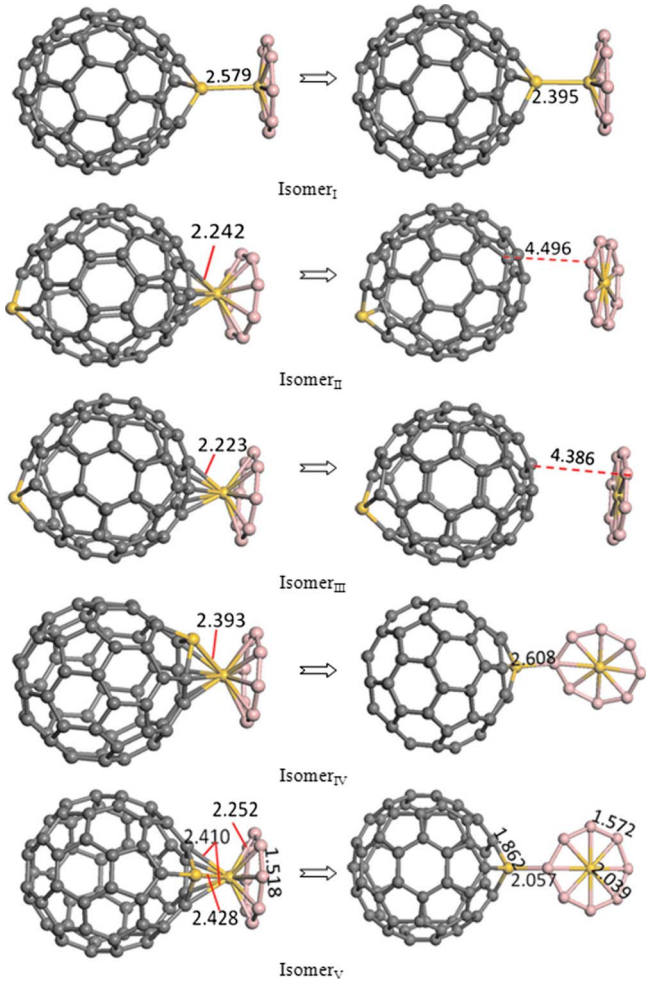

FIG. 5. (Color online) Initial (left column) and optimized (right column) structures of $C_{59}Si+B_8Si$. The labeled bond values are in angstrom (Å).

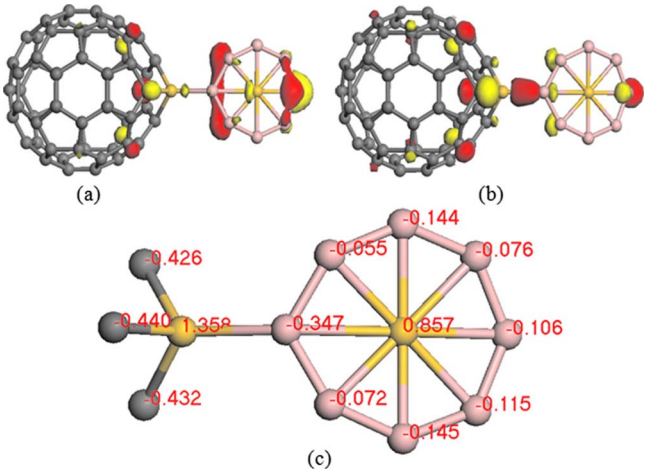

FIG. 6. (Color online) (a) HOMO, (b) LUMO, and (c) Mulliken charge distributions in the ground state of $B_8Si+C_{59}Si$.

tached to the Si site through the B site, as the Si site is positively charged while the B site is negatively charged. The electric dipole moment of $B_8Si+C_{59}Si$ is 0.655 D. Unlike $N_7Sc+C_{59}Si$, the HOMO and LUMO mainly come from the Si site and the molecular wheel [Figs. 6(a) and 6(b)]. The binding of the B_8Si molecule causes the charges to redistribute [Fig. 6(c)]. Thus, the Si site in $C_{59}Si$ becomes more positively charged, while Si site in B_8Si gets less positively charged.

E. Interaction of B_8Si+N_7Sc with $C_{59}Si$

We saw in the above that the binding of N_7Sc or B_8Si to $C_{59}Si$ enhances the anisotropy. It would be very interesting to see what will happen when both N_7Sc and B_8Si are introduced near the Si site in $C_{59}Si$. We have studied this in two different ways: first, interacting B_8Si with already formed $C_{59}Si+N_7Sc$ and second, interacting N_7Sc with already formed $C_{59}Si+B_8Si$.

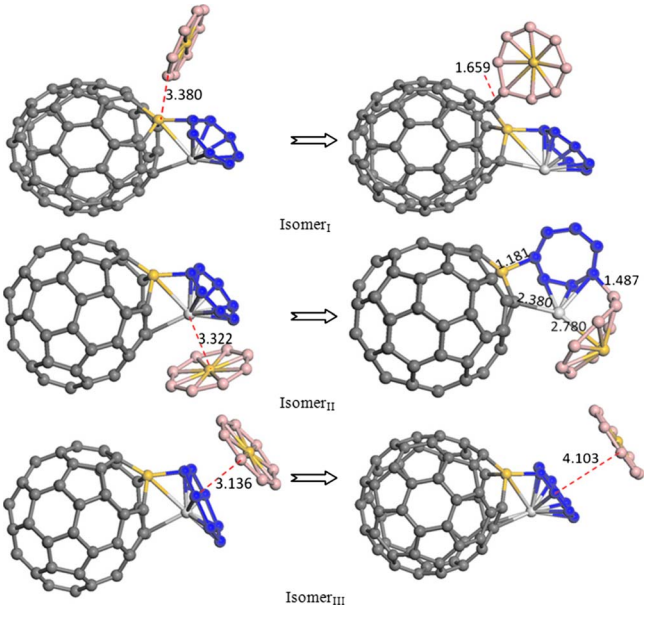

FIG. 7. (Color online) The initial (left column) and the optimized (right column) geometries of adding (B_8Si+N_7Sc) interacting with $C_{59}Si$.

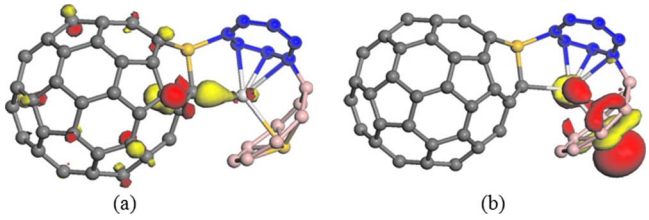

FIG. 8. (Color online) (a) HOMO and (b) LUMO in $C_{59}Si+N_7Sc+B_8Si$.

To determine the lowest energy structure of B_8Si molecular wheel interacting with $C_{59}Si+N_7Sc$, we used three different configurations (Fig. 7). In isomer$_I$ we placed the molecular wheel near the Si site. After optimization the binding occurs at C, which is adjacent to Si. The corresponding adsorption energy is 1.129 eV. When B_8Si is placed near Sc site (isomer$_{II}$), the optimized geometry shows that the binding is stronger, with an absorption energy of 3.286 eV. However, when the molecular wheel is placed on top of N_7Sc ring (isomer$_{III}$), no binding was seen. In Fig. 8 we plot the frontier orbitals. The HOMO is mainly from Si, while the LUMO is from the molecular wheel, a situation very different from the cases we discussed above.

To determine the lowest energy structure of N_7Sc interacting with $C_{59}Si+B_8Si$, we again used three different configurations (Fig. 9). Among these we found that the most stable configuration is isomer$_{II}$, with the absorption energy of 1.539 eV, where the binding is through Si and Sc between the B_8Si wheel and the N_7Sc ring. For the isomer$_I$ and isomer$_{III}$, the adsorption energies are 0.715 and 0.423 eV, respectively. In Fig. 10 we show the HOMO and LUMO for isomer$_{II}$. The anisotropy in the frontier orbitals can be clearly seen. Comparing isomer$_{II}$ in Fig. 7 with isomer$_{II}$ in Fig. 9, we found that the former is 1.747 eV lower in energy. Thus, the ultimate geometry of $C_{59}Si+B_8Si+N_7Sc$ depends upon which of the two molecules was introduced first. If both are introduced simultaneously, the optimized structure will lead to isomer$_{II}$ in Fig. 7 as the preferred structure purely on energetics ground. The increased anisotropy of $C_{59}Si+B_8Si+N_7Sc$ compared to earlier structures yields the highest electric dipole moment, namely, 7.935 D.

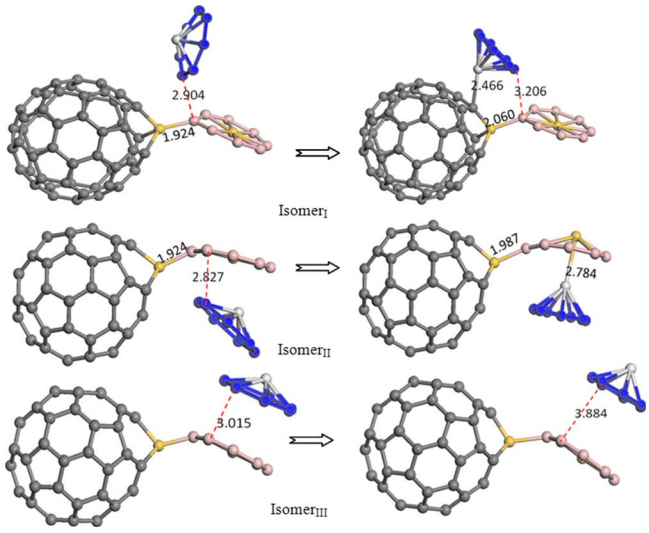

FIG. 9. (Color online) The isomers after adding N_7Sc to $B_8Si+C_{59}Si$.

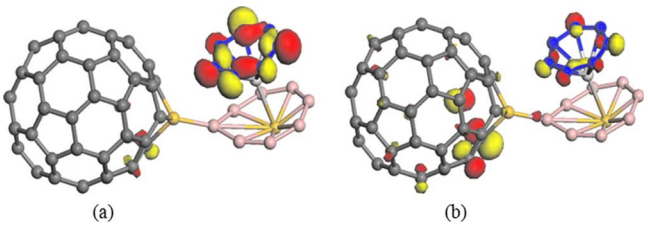

FIG. 10. (Color online) (a) HOMO and (b) LUMO in $C_{59}Si+B_8Si+N_7Sc$.

F. Hydrophobic-hydrophilic property of $C_{59}Si$ based structures

It is well known that the C_{60} fullerene is a very hydrophobic molecule. To demonstrate the anisotropy of $C_{59}Si$ induced by Si doping, we studied the interaction of a H_2O molecule with $C_{59}Si$. We introduced one H_2O molecule in $C_{59}Si$ supercell at two different sites: one at the opposite side of the Si with an initial distance of 2.300 Å away from a C atom [Fig. 11(a_1)] and the other at a site close to the Si atom [see Fig. 11(b_1)]. In the former case the interaction is found to be very weak with adsorption energy of 0.036 eV as expected, and the H_2O molecule is 3.533 Å away from the fullerene surface. In the latter case, on the other hand, the binding energy is 0.633 eV and the distance between H_2O and the Si atom is 1.920 Å. This shows that $C_{59}Si$ has a hydrophobic head and a hydrophilic tail.

The situation is different when a H_2O molecule was attached to $C_{59}Si+B_8Si+N_7Sc$ as shown in Fig. 12. In $isomer_I$, H_2O was placed near Sc with an initial distance of 2.300 Å. In the optimized structure the distance reduced to 2.206 Å, and the interaction is enhanced with an adsorption energy of 1.440 eV. When the H_2O molecule is placed at the Si site ($isomer_{II}$), the adsorption energy is 0.971 eV. When two H_2O molecules are introduced simultaneously to Sc and Si sites, the average binding energy is 1.151 eV. It is even possible to bind a third H_2O molecule next to Sc with an adsorption energy of 0.450 eV. On the other hand, when H_2O is placed on the other side ($isomer_{III}$), the adsorption energy is only 0.038 eV. We should point out that when we introduced a second H_2O molecule to $C_{59}Si:H_2O$ in Fig. 11(b_2), the adsorption was very weak. Thus, we see that the hydrophilic property of $C_{59}Si+B_8Si+N_7Sc$ is greatly improved, while its hydrophobic property remains unaffected. Increasing anisotropy of the Janus nanoparticles, therefore, enhances their hydrophobic and hydrophilic properties.

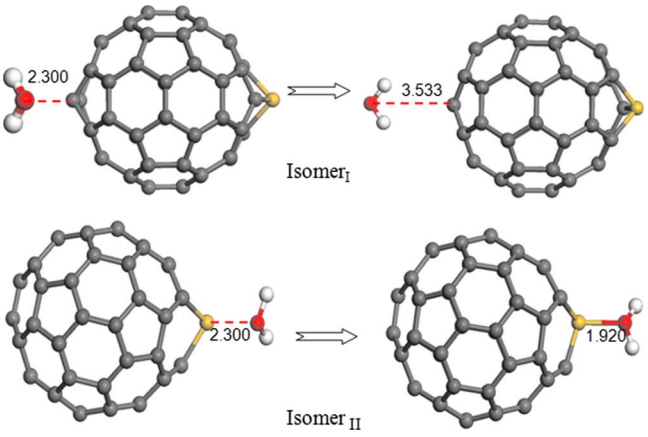

FIG. 11. (Color online) [(a_1) and (b_1)] Initial and [(a_2) and (b_2)] final structures of H_2O interacting with $C_{59}Si$.

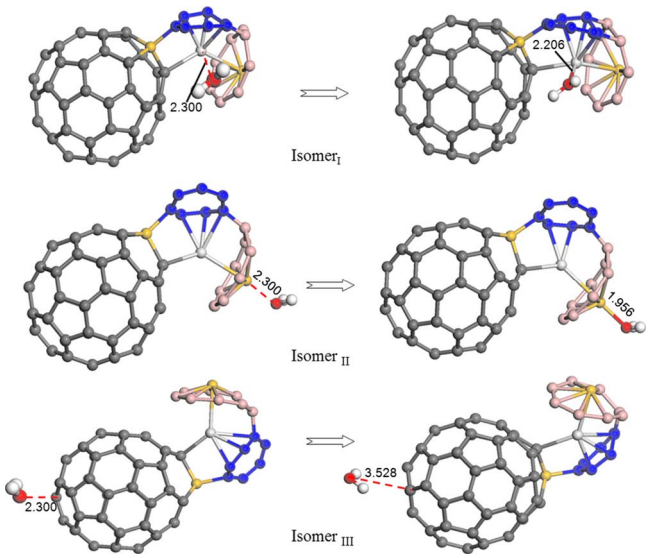

FIG. 12. (Color online) Interaction of H_2O with $C_{59}Si+N_7Sc+B_8Si$.

IV. SUMMARY

Based on our extensive calculations on $C_{59}Si$ interacting with N_7Sc and B_8Si, we have shown that heterofullerenes can be used to synthesize Janus-like nanostructures as substitutional doping can act as a seed for the anisotropic growth of the fullerene cage. The sites near the dopant become more reactive, so the anisotropic growth starts from the planted seed. The resulting anisotropy manifests in geometry, electronic structure, frontier orbital, hydrophobic-hydrophilic properties, and charge distribution. Especially, the dipole moment changes from 1.420 D in $C_{59}Si$ to 2.888 and 7.935 D in ($N_7Sc+C_{59}Si$) and ($N_7Sc+C_{59}Si+B_8Si$), respectively. $C_{59}Si$ has a hydrophobic head with a hydrophilic tail, and only one water molecule can be adsorbed at the Si site. On the other hand ($N_7Sc+C_{59}Si+B_8Si$) can attach more water molecules, thus enhancing its hydrophilicity. Its hydrophobic nature remains unaffected. In addition to $C_{59}Si$, other heterofullerenes including $C_{59}X$ (X=N,B,O,P,As,Ge,Ir) have already been synthesized in experiments.[28–34] These can also be used to grow anisotropic nanostructures. Recently, the stability of silicon-doped C_{60} dimers has been studied,[35] suggesting that Si-doped fullerenes can possibly be used as the basic units for constructing new fullerene-based polymers. We hope that the above finding as well as our results will motivate future experimental efforts for synthesizing fullerene-based Janus nanostructures and fullerene-based polymers.

ACKNOWLEDGMENTS

This work is partially supported by grants from the National Natural Science Foundation of China (Grant Nos. NSFC-10744006 and NSFC-10874007) and from the U.S. Department of Energy. The authors thank the crew of the Center for Computational Materials Science, the Institute for

Materials Research, Tohoku University (Japan), for their continuous support of the HITACHI SR11000 supercomputing facility.

[1] R. Klajn, K. J. M. Bishop, M. Fialkowski, M. Paszewski, C. J. Campbell, T. P. Gray, and B. A. Grzybowski, Science **316**, 261 (2007).
[2] S. C. Glotzer and M. J. Solomon, Nature Mater. **6**, 557 (2007).
[3] E. V. Shevchenko, D. V. Talapin, N. A. Kotov, S. O'Brien, and C. B. Murray, Nature (London) **439**, 55 (2006).
[4] A. van Blaaderen, Nature (London) **439**, 545 (2006).
[5] M. E. Leunissen, Nature (London) **437**, 235 (2005).
[6] K.-H. Roh, D. C. Matin, and J. Lahann, Nature Mater. **4**, 759 (2005).
[7] P. G. De Gennes, Rev. Mod. Phys. **64**, 645 (1992).
[8] T. Nisisako and T. Torii, Adv. Mater. (Weinheim, Ger.) **19**, 1489 (2007).
[9] A. Walther, X. Andre, M. Drechsler, V. Abetz, and A. H. E. Muller, J. Am. Chem. Soc. **129**, 6187 (2007).
[10] Z. Nie, W. Li, M. Seo, S. Xu, and E. Kumacheva, J. Am. Chem. Soc. **128**, 9408 (2006).
[11] T. Nisisako, T. Torii, and T. Takahashi, Adv. Mater. (Weinheim, Ger.) **18**, 1152 (2006).
[12] A. Perro, S. Reculusa, S. Ravaine, E. Bourgeat-Lami, and E. Duguet, J. Mater. Chem. **15**, 3745 (2005).
[13] S. C. Glotzer, Science **306**, 419 (2004).
[14] V. N. Paunov and O. J. Cayre, Adv. Mater. (Weinheim, Ger.) **16**, 788 (2004).
[15] Q. Sun, Q. Wang, P. Jena, and Y. Kawazoe, ACS Nano **2**, 341 (2008).
[16] S. Fuchs, A. Pla-Quintana, S. Mazeres, A. M. Caminade, and J. P. Majoral, Org. Lett. **10**, 4751 (2008).
[17] T. Kimura, T. Sigai, and H. Shinohara, Chem. Phys. Lett. **256**, 269 (1996).
[18] Q. Sun, Q. Wang, P. Jena, and Y. Kawazoe, Phys. Rev. Lett. **90**, 135503 (2003).
[19] Y. Wang and J. P. Perdew, Phys. Rev. B **44**, 13298 (1991).
[20] P. Blochl, Phys. Rev. B **50**, 17953 (1994).
[21] G. Kresse and J. Joubert, Phys. Rev. B **59**, 1758 (1999).
[22] J. Lu, Y. Luo, Y. Huang, X. Zhang, and X. Zhao, Solid State Commun. **118**, 309 (2001).
[23] R. B. Darzynkiewicz and G. E. Scuseria, J. Phys. Chem. A **101**, 7141 (1997).
[24] I. M. L. Billas, C. Massobri, M. Boero, M. Parrinello, W. Branze, N. Malinowski, M. Heinebrodt, and T. P. Martin, J. Chem. Phys. **111**, 6787 (1999).
[25] C. Ray, M. Pellarin, J. L. Lermé, J. L. Viallel, M. Broyer, X. Blase, P. Melinon, P. Keghelian, and A. Perez, Phys. Rev. Lett. **80**, 5365 (1998).
[26] L. Gagliardi and P. Pyykkö, J. Am. Chem. Soc. **123**, 9700 (2001).
[27] S. Li, C. Miao, J. Guo, and G. Ren, J. Am. Chem. Soc. **126**, 16227 (2004).
[28] T. Guo, C. Jin, and R. E. Smalley, J. Phys. Chem. **95**, 4948 (1991).
[29] J. C. Hummelen, B. Knight, J. Pavlovich, R. Gonzalez, and F. Wudl, Science **269**, 1554 (1995).
[30] T. Ohtsuki, K. Ohno, K. Shiga, Y. Kawazoe, Y. Maruyama, and K. Masumoto, J. Chem. Phys. **112**, 2834 (2000).
[31] W. Branz, I. M. L. Billas, K. Shiga, Y. Kawazoe, Y. Maruyama, and K. Masunoto, J. Chem. Phys. **109**, 3425 (1998).
[32] J. J. Stry and J. F. Garvey, Chem. Phys. Lett. **243**, 199 (1995).
[33] C. Möschel and M. Jansen, Z. Anorg. Allg. Chem. **625**, 175 (1999).
[34] J. M. Poblet, J. Muñoz, K. Winkler, M. Cancilla, A. Hayashi, C. B. Lebrilla, and A. L. Balch, Chem. Commun. (Cambridge) **6**, 493 (1999).
[35] P. A. Marcos, J. A. Alonso, and M. L. López, J. Chem. Phys. **126**, 044705 (2007).